



Contents lists available at ScienceDirect

## Journal of the Mechanics and Physics of Solids

journal homepage: [www.elsevier.com/locate/jmps](http://www.elsevier.com/locate/jmps)

## Hydration and swelling of dry polymers for wet adhesion

Xinyu Mao<sup>a</sup>, Hyunwoo Yuk<sup>a</sup>, Xuanhe Zhao<sup>a,b,\*</sup><sup>a</sup> Department of Mechanical Engineering, Massachusetts Institute of Technology, Cambridge, MA 02139, USA<sup>b</sup> Department of Civil and Environmental Engineering, Massachusetts Institute of Technology, Cambridge, MA 02139, USA

## ARTICLE INFO

## Article history:

Received 1 November 2019

Revised 1 January 2020

Accepted 1 January 2020

Available online 2 January 2020

## Keywords:

Hydration

Swelling

Dry polymer

Wet adhesion

## ABSTRACT

Whereas two dry surfaces can adhere to each other upon contact, it is challenging to form adhesion between two wet surfaces separated by interfacial water. A commonly used strategy for adhesion of wet surfaces such as wet tissues is to let adhesives such as monomers, macromers, polymers, and particles diffuse across the interfacial water and subsequently form physical and/or chemical crosslinking with the surfaces. In contrast, a recently developed strategy for wet adhesion is to make adhesives such as dry polymer networks quickly absorb the interfacial water and then crosslink with the surfaces. Since the absorption of interfacial water requires hydration and swelling of the dry polymer networks, understanding the physics and mechanics of this concurrent hydration and swelling process will potentially facilitate the design of future adhesives for wet adhesion. In this paper, we present a combined theoretical and experimental study on dry polymer networks that absorb interfacial water for wet adhesion. We observe that the absorption of interfacial water creates a sharp hydration front in the initially dry polymer network, where the hydrated part swells by further absorption of water and the un-hydrated part maintains in the dry state. We develop a quantitative model for the coupled hydration and swelling of polymer networks governed by the Case-I diffusion and validate the model with experimental data. We finally present a guideline for the design of dry polymer networks to achieve fast, stable, and tough adhesion with wet surfaces.

© 2020 Elsevier Ltd. All rights reserved.

## 1. Introduction

When two dry surfaces are brought into contact with each other (Fig. 1a), they can form instant adhesion due to mechanisms such as hydrogen bonds, physical entanglements, electrostatic and van der Waals interactions (Bartlett et al., 2012; Chaudhury, 1996; Chung and Chaudhury, 2005; Comyn, 2012; Creton, 2003; Lee, 2013; Long et al., 2010; Long and Hui, 2012; Yang et al., 2019). If interfacial water presents on one or both surfaces (Fig. 1b), the abovementioned interactions will be significantly hindered as the interfacial water separates molecules from the two surfaces (Lee et al., 2011; Petrone et al., 2015; Waite, 1987; Yuk et al., 2016a, 2016b, 2017; Zhao et al., 2017). Wet adhesion of surfaces with interfacial water, however, is of great significance in a broad range of biomedical and industrial applications such as bioadhesives for wet tissues and underwater glues (Annabi et al., 2015; Chung and Grubbs, 2012; Li et al., 2017).

A commonly used strategy for adhesion of wet surfaces such as wet tissues relies on a diffusion-based mechanism. Without loss of generality, let's consider that an adherend *A* is brought into contact with another adherend *B* covered with

\* Corresponding author.

E-mail address: [zhaox@mit.edu](mailto:zhaox@mit.edu) (X. Zhao).

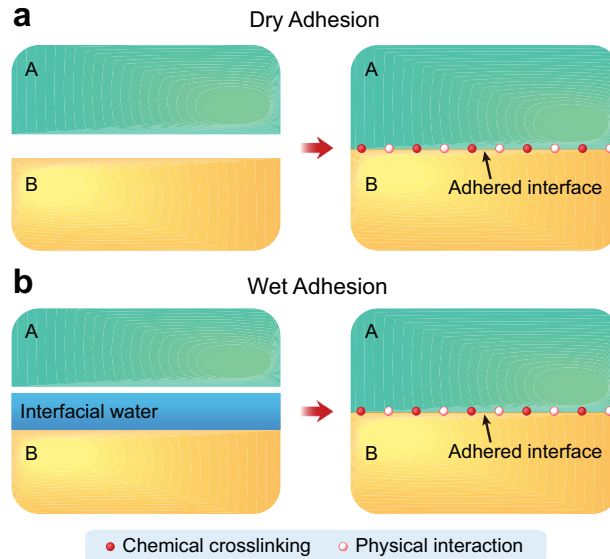


**Fig. 1.** Dry adhesion and wet adhesion. (a) Two adherends with dry surfaces are brought into contact, and an adhered interface is formed due to chemical crosslinking and/or physical interactions. (b) A dry adherend A is brought into contact with another adherend B covered with interfacial water. The adhered interface can also be formed by chemical crosslinking and/or physical interactions.

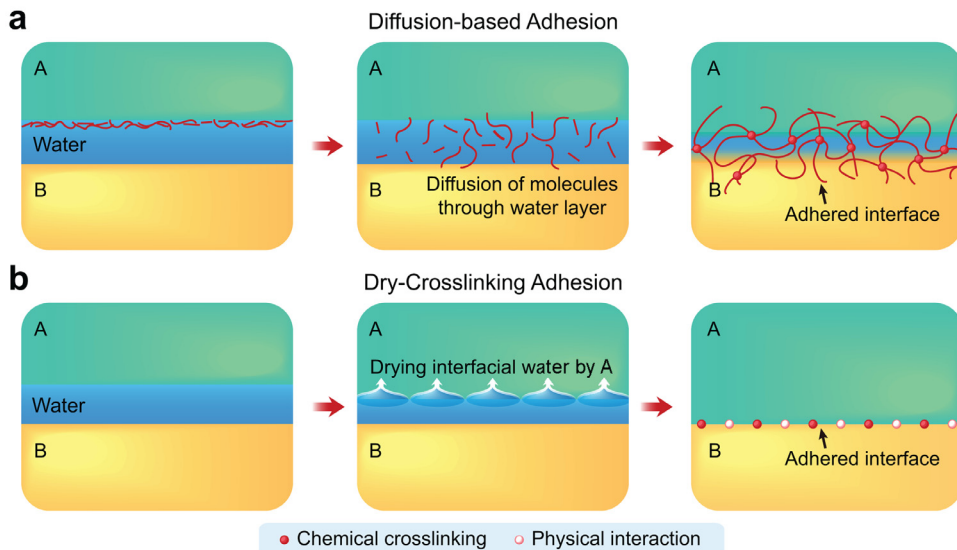


**Fig. 2.** Two mechanisms to achieve wet adhesion. (a) Diffusion-based mechanism. The adhesive components from the adherend A diffuse across the interfacial water and form an adhered interface with the adherend B by chemical and/or physical interactions. (b) Dry-crosslinking mechanism. The adherend A absorbs the interfacial water and then forms an adhered interface with the adherend B by chemical and/or physical interactions.

interfacial water (Fig. 2a). The adhesive components (e.g., monomers, macromers, polymers, and particles) from the adherend A can diffuse across the interfacial water to form physical and/or covalent crosslinking on the surface of or within the adherend B (Li et al., 2017; Meddahi-Pellé et al., 2014; Rose et al., 2014; Wang et al., 2007; Yang et al., 2018; Yuk et al., 2016a, 2016b, 2017). While this diffusion-based mechanism can bond wet surfaces, the diffusion of adhesive components typically requires a relatively long time, because of the low diffusivity of large molecules (Rouse, 1953; Zimm, 1956). For example, existing commercially available bioadhesives usually take a few minutes to adhere to wet tissues (Quinn, 2005; Yuk et al., 2019). Recently developed tough hydrogel adhesives (Li et al., 2017) and topological adhesion (Yang et al., 2018) require steady compression of adherends for 5 to 30 min to form stable adhesion.

Recently, we have proposed a new strategy for fast and strong adhesion of wet surfaces named as the dry-crosslinking mechanism (Yuk et al., 2019). Instead of diffusing adhesive components, the adherend A can quickly absorb the interfacial water, contact the surface of the adherend B, and subsequently form both physical interactions and covalent crosslinking

on the interface (Fig. 2b). As an embodiment of the dry-crosslinking mechanism, a double-sided tape of dry hydrophilic polymer networks (i.e., adherend A) forms adhesion on diverse wet tissues (i.e., adherend B) within 5 s, giving stable and high interfacial toughness up to 1000 J/m<sup>2</sup> over multiple days (Yuk et al., 2019). While the dry-crosslinking mechanism (Fig. 2b) demonstrates advantages over the diffusion-based mechanism (Fig. 2a) for wet adhesion, the physics and mechanics for absorbing interfacial water are still not fully understood. A quantitative understanding of the dry-crosslinking mechanism will potentially facilitate the rational design of future adhesives for wet adhesion. Since dry hydrophilic polymer networks have been widely used for the implementation of the dry-crosslinking mechanism (Yuk et al., 2019), we will choose them as a model material to study the physics and mechanics of absorbing interfacial water in this paper. Unlike wet polymeric hydrogels, which swell upon absorption of water, a dry hydrophilic polymer network undergoes both hydration and swelling when it is in contact with water. Thus, studying the kinetics of coupled hydration and swelling of dry polymer networks is essential for the quantitative understanding of the absorption of interfacial water in the dry-crosslinking mechanism.

The hydration kinetics of dry polymers have been extensively studied over the past decades (Ji and Ding, 2002; Peppas and Colombo, 1997; Thomas and Windle, 1982). The hydration of a dry polymer network generally creates a sharp and moving hydration front, which separates the polymer network into the hydrated and dry parts (Alfrey et al., 1966; Hartley, 1946; Lasky et al., 1988; Thomas and Windle, 1982). Since the hydration is associated with the diffusion of water, three categories of diffusion kinetics, i.e., Case-I diffusion, Case-II diffusion, and anomalous diffusion, have been used to describe the hydration behaviors (Crank, 1979). As the most common category, Case-I diffusion has a negligible time scale for polymer relaxation compared with solvent diffusion, and thus the Fick's laws of diffusion are employed to describe the hydration process, in which the hydration front advances by a distance proportional to the square root of time. In contrast, the time scale for Case-II diffusion is governed by polymer relaxation, and the distance that the hydration front propagates shows a linear scaling relation with time in Case-II diffusion (Thomas and Windle, 1982). Anomalous diffusion lies between the above two extreme cases (Crank, 1979).

Crank established a classical theory for the sharp hydration front in the Case-I scenario (Crank, 1953, 1951). It was assumed that the sharp hydration front is associated with a sharp variation in the diffusivity of water molecules in the hydrated and dry parts. By using a step function for the relation between the diffusivity and the water concentration (e.g., Fig. 4b), Crank provided an analytical solution for the position of the sharp penetrant front as a function of time in a one-dimensional model. However, Crank's model did not consider the swelling of the hydrated polymers. While Wang and Kwei considered the swelling of the hydrated part of the polymer network (Frisch et al., 1969; Kwei and Zupko, 1969; Wang et al., 1969), their model assumed a uniform swelling ratio in the hydrated part. Furthermore, some models were developed for the inhomogeneous swelling and large deformation of wet polymeric gels (Anand et al., 2009; Bouklas and Huang, 2012; Chester et al., 2015; Chester and Anand, 2010; Doi, 2009; Hong et al., 2008; Yoon et al., 2010), but these models did not consider the hydration of polymer networks, only applicable to wet gels.

In this paper, we present a combined theoretical and experimental study on the coupled hydration and inhomogeneous swelling of dry polymeric networks. We observe that the absorption of water indeed creates a sharp and moving hydration front in the initially dry polymer network, where the hydrated part swells by further absorption and the un-hydrated part maintains in the dry state. We develop a quantitative model for the coupled hydration and inhomogeneous swelling of dry polymer networks following Case-I diffusion and provide a set of results on the hydration and swelling behavior of dry polymer networks by analytically and numerically solving the model. After validating the model with experimental data, we finally present a guideline for the design of dry polymer networks to achieve fast, stable, and tough adhesion with wet surfaces.

The remaining part of the paper is organized as follows. In Section 2, we develop the theoretical model for the coupled hydration and inhomogeneous swelling of dry polymer networks. Section 3 provides the asymptotic solutions for two limiting cases, in which either the hydration or diffusion kinetics is much faster than the other one. Section 4 provides numerical solutions for general cases, in which the hydration and diffusion kinetics are on the same order. Our model is experimentally validated in Section 5. In Section 6, we will present the guideline for the design of dry adhesives. Section 6 also discusses on the time scales for the diffusion-based and dry-crosslinking mechanisms, demonstrating the merit of the dry-crosslinking mechanism in terms of achieving faster adhesion. Section 7 gives the concluding remarks of the paper.

## 2. Theoretical model

### 2.1. Kinematics of the hydration and swelling process

We first provide a qualitative overview of the hydration and swelling of the dry adhesive in the form of a layer of a dry hydrophilic polymer network (Yuk et al., 2019). One surface of the dry polymer network is bonded on a rigid substrate (Fig. 3a). As the other surface of the dry polymer network is in contact with water, a sharp hydration front advances within the polymer, dividing it into a hydrated part and a dry part (Fig. 3b). Meanwhile, the hydrated part of the polymer further swells by absorbing more water. As the hydration front reaches the bonded surface, the polymer network becomes fully hydrated. The polymer continues to swell as a common hydrogel (Fig. 3c), and eventually reaches an equilibrium swollen state (Fig. 3d).

We define the dry state of the polymer network as the reference state (Fig. 3a), which is isotropic and stress-free following the convention of previous models for gels (Bouklas and Huang, 2012; Hong et al., 2008; Yoon et al., 2010). Due to

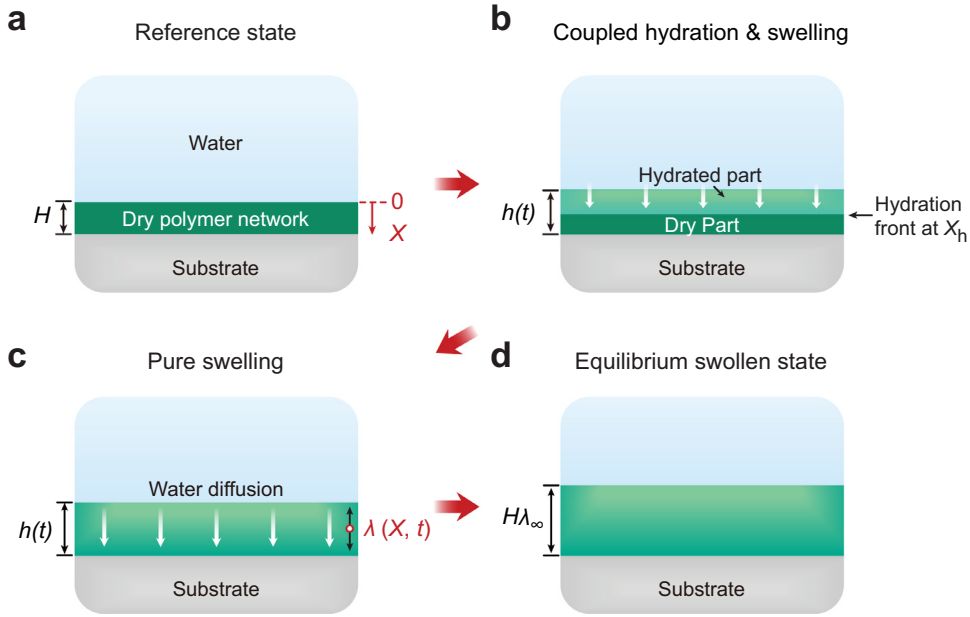


**Fig. 3.** The hydration and swelling process of a dry polymer network. (a) A dry polymer network with a thickness of  $H$  is bonded on a rigid substrate. Coordinate  $X$  is defined from the top surface of the polymer network, which is in direct contact with water. The initial dry state is regarded as the reference state. (b) The dry polymer network first undergoes a coupled hydration and swelling process. The water migrates into the polymer network and forms a sharp hydration front with a coordinate of  $X_h$ , which separates the polymer network into a hydrated part and a dry part. As the hydration front moves towards the substrate, the hydrated part further swells in the thickness direction. (c) After becoming fully hydrated, the polymer network undergoes a pure swelling process. (d) At the equilibrium state, the polymer network achieves an equilibrium thickness of  $H\lambda_\infty$ .

the planar geometry of the dry polymer layer and the constraint by the substrate, the polymer can only swell along the thickness direction. Thus, the hydration and swelling of the polymer can be regarded as a one-dimensional process. A point in the polymer network is denoted by its coordinate  $X$  along the thickness direction in the reference state (Fig. 3a). It should be noted that if the swelling ratio of the polymer is above a certain value, the creasing instability can occur on the surface of the polymer (Hohlfeld and Mahadevan, 2012; Hong et al., 2009). However, since the creasing instability will be localized at a few locations on the surface of the polymer, it is expected that the creasing instability does not significantly affect the kinetics of water absorption by the polymer.

In the reference state, the dry polymer network has an initial thickness of  $H$ . The thickness of the polymer network in the current state at time  $t$  is denoted by  $h(t)$ . Due to the constraint of the substrate, the principal stretches of the polymer network along two in-plane directions maintain to be 1 throughout the hydration and swelling process. The principal stretch of a point in the polymer network along the out-of-plane (thickness) direction in the current state is denoted by  $\lambda(X, t)$ , which is a function of the point's coordinate  $X$  and the current time  $t$  (Fig. 3c). Defining the swelling ratio of a point as the point's volume in the current state over its volume in the reference state, the swelling ratio is equal to the out-of-plane principal stretch of the point  $\lambda(X, t)$ . In the equilibrium swollen state, all points in the polymer network have an equilibrium swelling ratio of  $\lambda_\infty$  in the thickness direction.

Furthermore, we define the water concentration of a point in the polymer network as the number of water molecules per unit volume of the point in the reference state  $C(X, t)$ , which is a function of the point's coordinate  $X$  and the current time  $t$ . The volume of a point in the polymer network is taken to be equal to the summation of the volumes of dry polymer network and water at the point (Flory, 1953; Hong et al., 2008), which leads to the relation,

$$1 + \nu C = \lambda \quad (2.1)$$

where  $\nu$  is the volume per water molecule. In the equilibrium swollen state, all points in the polymer network have an equilibrium water concentration of  $C_\infty$ , and Eq. (2.1) gives

$$1 + \nu C_\infty = \lambda_\infty \quad (2.2)$$

## 2.2. Thermodynamics of the swollen polymer network

Next, we discuss the thermodynamics of the polymer network during the swelling process. The equilibrium swollen state of the polymer network results from a balance of the Helmholtz free energies of stretching polymer chains and mixing polymer chains with water (Flory and Rehner, 1943). The nominal Helmholtz free energy function  $W$ , defined as the Helmholtz

free energy per unit volume of the polymer network in the reference state, is taken as a function of the out-of-plane principal stretch  $\lambda$  and the water concentration  $C$  per unit volume of the reference state. The out-of-plane nominal stress  $s$  and the chemical potential of a water molecule in the polymer  $\mu$  are calculated as the partial derivatives of  $W$  with respect to  $\lambda$  and  $C$ , respectively (Flory, 1953; Hong et al., 2008),

$$s = \frac{\partial W(\lambda, C)}{\partial \lambda} \quad (2.3)$$

$$\mu = \frac{\partial W(\lambda, C)}{\partial C} \quad (2.4)$$

The polymer network is taken to follow the Flory-Rehner Helmholtz free energy function (Flory, 1953; Hong et al., 2008),

$$W(\lambda, C) = W_s(\lambda) + W_m(C) + \Pi(1 + \nu C - \lambda) \quad (2.5)$$

where  $W_s(\lambda)$  and  $W_m(C)$  are contributions from stretching the polymer network and mixing of polymer chains and water to the Helmholtz free energy, respectively. The term  $\Pi(1 + \nu C - \lambda)$  reinforces the assumption of molecular incompressibility Eq. (2.1), where  $\Pi$  is a Lagrange multiplier. For the one-dimensional problem,  $W_s(\lambda)$  and  $W_m(C)$  are taken to follow the Flory-Rehner free energy function (Flory, 1953, 1942; Hong et al., 2008; Huggins, 1941)

$$W_s(\lambda) = \frac{1}{2} N k_B T (\lambda^2 - 1 - 2 \ln \lambda) \quad (2.6)$$

$$W_m(C) = -\frac{k_B T}{\nu} \left[ \nu C \ln \left( 1 + \frac{1}{\nu C} \right) + \frac{\chi}{1 + \nu C} \right] \quad (2.7)$$

where  $N$  is the number of polymer chains per unit volume of the polymer network in the reference state,  $k_B$  is the Boltzmann constant,  $T$  is the absolute temperature,  $\nu$  is the volume per water molecule, and  $\chi$  is the Flory solvent-polymer interaction parameter.

Substituting Eqs. (2.5)–(2.7) into Eqs. (2.3) and (2.4), we can obtain that

$$s = N k_B T (\lambda - \lambda^{-1}) - \Pi \quad (2.8)$$

$$\mu = k_B T \left[ \ln \frac{\lambda - 1}{\lambda} + \frac{1}{\lambda} + \frac{\chi}{\lambda^2} \right] + \Pi \nu \quad (2.9)$$

In the absence of body forces, the mechanical equilibrium condition  $\partial s / \partial X = 0$  and the traction-free boundary condition  $s(X=0) = 0$  require that  $s = 0$  in Eq. (2.8), which gives  $\Pi = N k_B T (\lambda - \lambda^{-1})$ . At the equilibrium swollen state, the chemical potential of water molecules in the polymer network is equal to that of the interfacial water  $\mu_0$ , which is taken to be 0, and thus  $\mu = 0$  in Eq. (2.9). Therefore, the equilibrium swelling ratio (or out-of-plane stretch) of the polymer network  $\lambda_\infty$  can be solved from the following equation,

$$\ln \frac{\lambda_\infty - 1}{\lambda_\infty} + \frac{1}{\lambda_\infty} + \frac{\chi}{\lambda_\infty^2} + N \nu \left( \lambda_\infty - \frac{1}{\lambda_\infty} \right) = 0 \quad (2.10)$$

### 2.3. Kinetics of Case-I hydration and swelling

The transportation of water molecules throughout the polymer network is taken to follow Crank's diffusion model (Crank, 1951, 1979; Frisch et al., 1969). The water molecules diffuse in the hydrated part of the polymer network as in common hydrogels, which is featured with a relatively high diffusivity. By contrast, the diffusion of water molecules in the dry part can be negligibly slow, corresponding to a diffusivity many orders of magnitudes lower than the diffusivity in the hydrated part (Frisch et al., 1969; Windle, 1985). As the water molecules reach the hydration front, the initially dry polymer network in the glassy state begins to transform into a hydrated polymer network in the rubbery state, which is accompanied with a dramatic increase in the water diffusivity in the hydrated polymer network (Frisch et al., 1969) (Fig. 4a). This transition of the polymer network from the glassy state to the rubbery state is due to the reduction of the polymer network's glass transition temperature  $T_g$  during hydration. A simplified expression for  $T_g$  reads as (Frisch et al., 1969; Kelley and Bueche, 1961):

$$T_g = \frac{\alpha_1 T_{g1} + \alpha_2 \nu C T_{g2}}{\alpha_1 + \alpha_2 \nu C} \quad (2.11)$$

where  $\nu$  is the volume of a water molecule,  $C$  is the number of water molecules per unit volume of the polymer in the reference state,  $T_{g1}$  and  $T_{g2}$  are the glass transition temperature of the polymer and the melting point of the solvent, respectively, and  $\alpha_1$  and  $\alpha_2$  are the thermal expansion coefficients of the polymer and the solvent, respectively. The melting point  $T_{g2}$  of a typical solvent such as water is much lower than the glass transition temperature  $T_{g1}$  of a typical polymer.

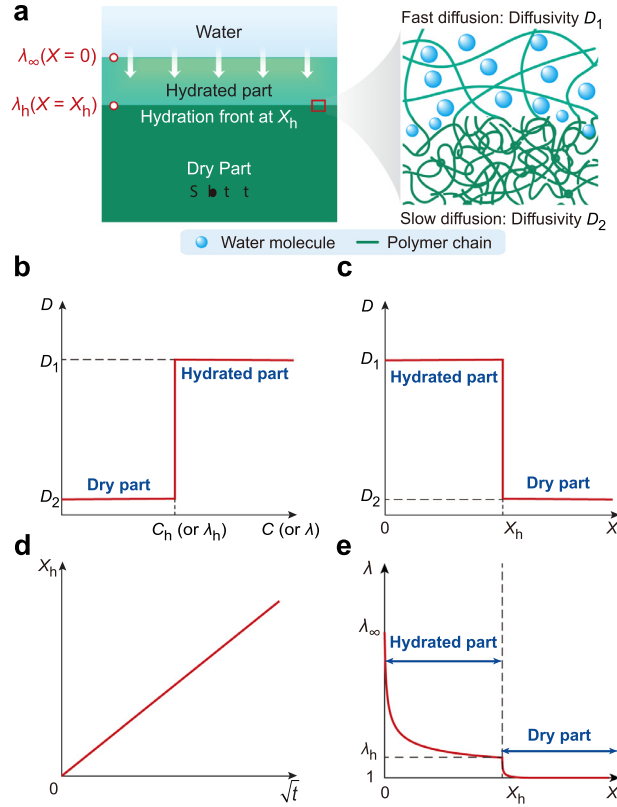


**Fig. 4.** Coupled hydration and swelling of a dry polymer network as a semi-infinite medium. (a) The hydration front at  $X = X_h$  corresponds to a transition from the relatively fast diffusion ( $D = D_1$ ) to the relatively slow diffusion ( $D = D_2$ ,  $D_2 \ll D_1$ ). The magnified view shows more water molecules present at the hydrated side of the hydration front, whereas water concentration decreases sharply at the dry side of the hydration front. (b) Diffusivity  $D$  as a step function of water concentration  $C$  or swelling ratio  $\lambda$ , where  $C_h$  or  $\lambda_h$  denotes the critical water concentration or the critical swelling ratio at the hydration front, respectively. (c) Distribution of diffusivity  $D$  in the thickness direction of the polymer network. (d) The coordinate of the hydration front  $X_h$  in the polymer network versus  $\sqrt{t}$ . (e) Distribution of swelling ratio  $\lambda$  in the thickness direction of the polymer network, where  $\lambda_\infty$  denotes the equilibrium swelling ratio at the boundary in contact with water.

Therefore, when the solvent concentration  $C$  reaches a critical value  $C_h$  or the swelling ratio  $\lambda$  reaches a critical value  $\lambda_h$  based on Eq. (2.1),  $T_g$  of the hydrated polymer network reduces below the ambient temperature, giving rise to the rubbery state of the hydrated polymer.

During the hydration and swelling process, the transportation of water molecules throughout the polymer network can be taken to follow the general Darcy's law (Bouklas and Huang, 2012; Hong et al., 2008; Yoon et al., 2010),

$$J = -M \frac{\partial \mu}{\partial X} \quad (2.12)$$

where the nominal flux of water  $J$  is the number of water molecules crossing per unit area in the reference state per unit time (Hong et al., 2008). The nominal mobility  $M$  depends on the kinetics of the diffusion of water molecules, which can be expressed as (Bouklas and Huang, 2012; Hong et al., 2008; Yoon et al., 2010)

$$M = \frac{D}{\nu k_B T} \lambda^{-2} (\lambda - 1) \quad (2.13)$$

where  $D$  is the diffusivity of water molecules in the polymer network. To capture the dramatic variation in the diffusivity at the hydration front, we model the diffusivity  $D$  as a step function of the swelling ratio  $\lambda$ , where a critical swelling ratio  $\lambda_h$  corresponds to the critical water concentration  $C_h$  for hydrating the dry polymer network (Crank, 1979, 1951; Frisch et al., 1969) (Fig. 4b). For a swelling ratio greater than  $\lambda_h$ , i.e., in the hydrated part, the diffusivity takes a value  $D_1$ , the same as the diffusivity in a swollen polymer network. For a swelling ratio lower than  $\lambda_h$ , i.e., in the dry part, the diffusivity takes a much lower value of  $D_2$  ( $D_1 \gg D_2 \approx 0$ ) (Fig. 4b, c, and e).

Before developing a kinetics model for a polymer network with a finite thickness, we first consider the polymer network as a semi-infinite medium (Fig. 4a). For the hydrated part, by substituting Eqs. (2.9) and (2.12)–(2.13) into the Fick's second



law, i.e.,  $\partial C/\partial t = -\partial J/\partial X$ , the evolution of the swelling ratio  $\lambda$  at each point of the hydrated part is given by (Bouklas and Huang, 2012)

$$\frac{\partial \lambda}{\partial t} = D_1 \frac{\partial}{\partial X} \left[ \xi(\lambda) \frac{\partial \lambda}{\partial X} \right] \tag{2.14}$$

where

$$\xi(\lambda) = \frac{1}{\lambda^4} - \frac{2\chi(\lambda - 1)}{\lambda^5} + N\nu \frac{(\lambda - 1)(\lambda^2 + 1)}{\lambda^4} \tag{2.15}$$

Note that Eqs. (2.14)–(2.15) take the same form for the constrained swelling of polymeric gels (Bouklas et al., 2015; Bouklas and Huang, 2012). Because the surface in contact with water is in the equilibrium swollen state, and the hydration front corresponds to the critical swelling ratio  $\lambda_h$ , the boundary conditions for Eq. (2.14) are expressed as

$$\begin{aligned} \lambda(X = 0, t \geq 0) &= \lambda_\infty \\ \lambda(X = X_h, t \geq 0) &= \lambda_h \end{aligned} \tag{2.16}$$

The kinetics in the dry part is subject to the same rule as the hydrated part, with a negligibly low diffusivity of  $D_2$ . Thus, the evolution equation for  $\lambda$  in the dry part reads as

$$\frac{\partial \lambda}{\partial t} = D_2 \frac{\partial}{\partial X} \left[ \xi_g(\lambda) \frac{\partial \lambda}{\partial X} \right] \tag{2.17}$$

where

$$\xi_g(\lambda) = \frac{1}{\lambda^4} - \frac{2\chi_g(\lambda - 1)}{\lambda^5} + N_g\nu \frac{(\lambda - 1)(\lambda^2 + 1)}{\lambda^4} \tag{2.18}$$

with  $N_g$  and  $\chi_g$  being the effective chain density and Flory solvent-polymer interaction parameter of the dry polymer network, respectively. As  $D_2 \rightarrow 0$ ,  $\xi_g(\lambda) = 1$  in Eq. (2.17) due to the negligible swelling in the dry polymer. To solve Eq. (2.17), the critical swelling ratio at the hydration front and the non-swelling behavior at infinity require

$$\begin{aligned} \lambda(X = X_h, t \geq 0) &= \lambda_h \\ \lambda(X = +\infty, t \geq 0) &= 1 \end{aligned} \tag{2.19}$$

Additionally, the flux of water holds constant at the hydration front on both sides, namely

$$D_1 \frac{\partial \lambda}{\partial X} \Big|_{X \rightarrow X_h^-} = D_2 \frac{\partial \lambda}{\partial X} \Big|_{X \rightarrow X_h^+} \tag{2.20}$$

Assuming  $\chi$  and  $N$  are material constants for the given polymer network,  $\lambda$  can be expressed as a function of a series of variables from Eqs. (2.14) – (2.20):

$$\lambda = F(t, X, D_1, D_2, X_h) \tag{2.21}$$

Note that  $\lambda_h$ , an intrinsic physical parameter of the model, is not included in Eq. (2.21) for later algebraic convenience, because  $\lambda_h$  can be determined from other variables in the function  $F$ . We can obtain a dimensionless form for Eq. (2.21) based on the Buckingham  $\pi$  theorem (Buckingham, 1914):

$$\lambda = F_1 \left( \frac{X}{X_h}, \frac{X_h^2}{D_1 t}, \frac{X_h^2}{D_2 t} \right) \tag{2.22}$$

We further introduce a hydration coefficient  $k_h = X_h/t^{1/2}$ , which characterizes the advancing speed of the hydration front within the polymer network. Thus, Eq. (2.22) is equivalent to

$$\lambda = F_1 \left( \bar{X}, \frac{k_h^2}{D_1}, \frac{k_h^2}{D_2} \right) \tag{2.23}$$

with dimensionless coordinate  $\bar{X} = X/X_h = X/(k_h t^{1/2})$ . Given that  $k_h^2/D_1$  and  $k_h^2/D_2$  are known material parameters, Eq. (2.23) implies that  $\lambda$  is solely a function of  $\bar{X}$ , i.e.,  $\lambda = \lambda(\bar{X})$ . Since  $X$  and  $t$  merge into a single parameter  $\bar{X}$ ,  $\lambda(\bar{X})$  has a self-similar solution for the problem.

By applying the chain rule, we transform the governing equation for the hydrated part, Eq. (2.14), into a dimensionless form:

$$-\frac{1}{2} \bar{X} \frac{d\lambda}{d\bar{X}} = \frac{D_1}{k_h^2} \frac{d}{d\bar{X}} \left( \xi(\lambda) \frac{d\lambda}{d\bar{X}} \right) \tag{2.24}$$

Eq. (2.24) is rearranged to be a nonlinear second-order ordinary differential equation

$$\frac{d^2 \lambda}{d\bar{X}^2} + f(\lambda) \left( \frac{d\lambda}{d\bar{X}} \right)^2 + g(\lambda) \frac{k_h^2}{D_1} \bar{X} \frac{d\lambda}{d\bar{X}} = 0 \tag{2.25}$$

where  $f(\lambda) = \xi'(\lambda)/\xi(\lambda)$  and  $g(\lambda) = 1/[2\xi(\lambda)]$ . The boundary conditions in Eq. (2.16) are equivalent to

$$\begin{aligned}\lambda(\bar{X} = 0) &= \lambda_\infty \\ \lambda(\bar{X} = 1) &= \lambda_h\end{aligned}\quad (2.26)$$

Similarly, in the dry part, the dimensionless evolution equation for  $\lambda$  reads:

$$\frac{d^2\lambda}{d\bar{X}^2} + f(\lambda)\left(\frac{d\lambda}{d\bar{X}}\right)^2 + g(\lambda)\frac{k_h^2}{D_2}\bar{X}\frac{d\lambda}{d\bar{X}} = 0 \quad (2.27)$$

with boundary conditions

$$\begin{aligned}\lambda(\bar{X} = 1) &= \lambda_h \\ \lambda(\bar{X} = +\infty) &= 1\end{aligned}\quad (2.28)$$

Eq. (2.20) is equivalent to

$$D_1 \frac{\partial \lambda}{\partial \bar{X}} \Big|_{\bar{X} \rightarrow 1^-} = D_2 \frac{\partial \lambda}{\partial \bar{X}} \Big|_{\bar{X} \rightarrow 1^+} \quad (2.29)$$

Although the above derivations are under the assumption of an infinite thickness  $H$  for the polymer network, they are also applicable for a finite thickness  $H$  if  $D_2 \rightarrow 0$ . As  $D_2 \rightarrow 0$ , the swelling ratio reduces sharply from  $\lambda_h$  to 1 at the hydration front. Therefore, the entire dry part has a constant swelling ratio of 1, regardless of the value of  $H$ .

Notably, in addition to the step function, there can be other forms of functions for the relation between  $D$  and  $C$  (or  $\lambda$ ). For example,  $D = D_1/(1 - \alpha C/C_\infty)$  and  $D = D_1 \exp(\beta C)$ , where  $\alpha$  and  $\beta$  are constants (Crank, 1979). Eventually, these functions should give the same set of kinetic parameters: the diffusivity in the swollen polymer network  $D_1$  and hydration coefficient  $k_h$ , both of which can be experimentally measured.

For a general problem on the hydration and swelling of a polymer,  $N$  and  $\chi$  are usually given as the measurable thermodynamic parameters of the polymer, and  $D_1$  and  $k_h$  as the measurable kinetic parameters of the polymer.  $D_2$  is usually set to be much lower than  $D_1$  by several orders of magnitude. The intrinsic physical parameter  $\lambda_h$  (or  $C_h$ ) can be numerically determined with the measured  $D_1$  and  $k_h$ . The kinetics of the hydration and swelling can be solved as follows:

When  $t < \sqrt{H/k_h}$ , the polymer network undergoes the coupled hydration and swelling process (Fig. 3b). The critical swelling ratio  $\lambda_h$  and the distribution of swelling ratio  $\lambda(\bar{X})$  can be obtained by solving Eqs. (2.25)–(2.29). Due to the complexity of  $f(\lambda)$  and  $g(\lambda)$ , we can numerically solve the problem with an infinitesimal but nonzero  $D_2$ . Furthermore, to bypass the difficulty of having a boundary condition at infinity for Eq. (2.28), a coordinate transformation  $\bar{Y} = 1/\bar{X}$  can be performed to reformulate Eqs. (2.27)–(2.29) on the interval of  $[0, 1]$ .

When  $t > \sqrt{H/k_h}$ , the polymer network undergoes the pure swelling process (Fig. 3c). The diffusivity in the fully hydrated polymer network is taken to be the same as the diffusivity in the hydrated part during the coupled hydration-swelling process. Thus, the kinetics of water transportation in the polymer network is governed by Eqs. (2.14) – (2.15). We set the equilibrium boundary condition for the top surface of the polymer network,

$$\lambda(X = 0, t > \sqrt{H/k_h}) = \lambda_\infty \quad (2.30)$$

For the surface bonded to the rigid substrate, the zero-flux boundary condition requires that

$$\frac{\partial \lambda}{\partial \bar{X}} \Big|_{X=H, t > \sqrt{H/k_h}} = 0 \quad (2.31)$$

Additionally, the initial condition for the pure swelling stage is obtained from the solution of Eq. (2.25) at  $t = \sqrt{H/k_h}$ . The evolution of  $\lambda$  during the pure swelling stage can be numerically solved based on the finite difference method (Bouklas and Huang, 2012).

### 3. Asymptotic solutions for limiting cases

As discussed above, water transportation in the dry polymer network shows two competing phenomena, namely hydration and swelling. The speed of hydration and swelling are characterized by the hydration coefficient  $k_h$  and diffusivity  $D_1$ , respectively. Here, we employ the dimensionless parameter  $k_h^2/D_1$  to quantify the relative importance of hydration over diffusion. As  $k_h^2/D_1$  varies from zero to infinity, the water transportation behavior in the polymer network will vary correspondingly. In this section, we discuss on two limiting cases, i.e.,  $k_h^2/D_1 \rightarrow \infty$  and  $k_h^2/D_1 \rightarrow 0$ . For each case, we will show the asymptotic results on how the thickness of the polymer network increases over time.

For the limiting case of an infinite hydration speed, i.e.,  $k_h^2/D_1 \rightarrow \infty$ , Fig. 5a schematically illustrates the hydration and swelling of a dry polymer network with thickness  $H$ . Due to the infinite hydration speed, the polymer network hydrates instantaneously in contact with water, and thereafter the kinetics is governed by pure swelling. At  $t = 0^+$ , the polymer network becomes fully hydrated, yet the thickness remains to be  $H$ . Subsequently, water continuously migrates through the



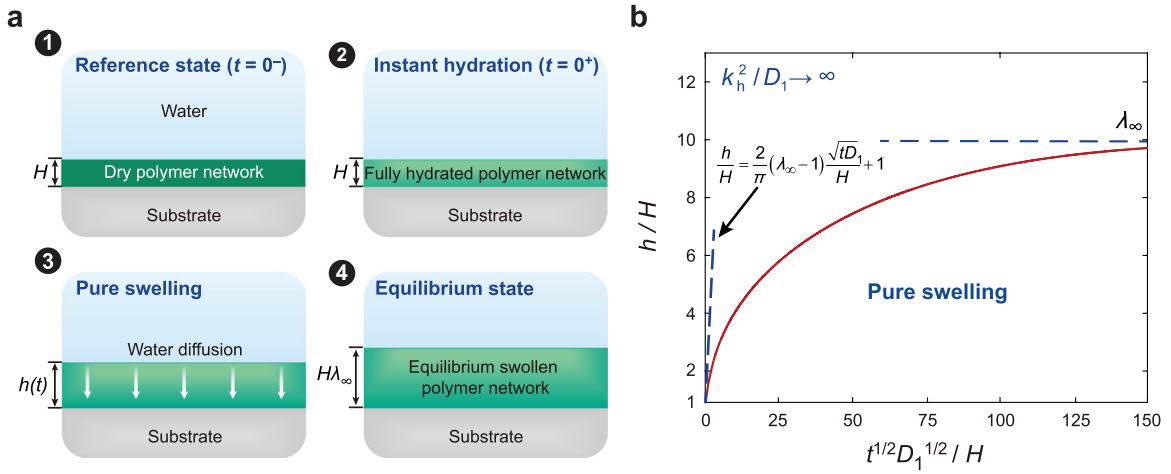


**Fig. 5.** A limiting case of an infinite hydration speed. (a) Schematic illustrations for the swelling of a dry polymer network with an infinite hydration coefficient  $k_h$  ( $k_h^2/D_1 \rightarrow \infty$ ). The dry polymer network with thickness  $H$  is bonded to a rigid substrate. At the instant of the introduction of water, the polymer network becomes fully hydrated with no change in the thickness. Then, the polymer network undergoes the pure swelling stage and reaches a thickness of  $H\lambda_\infty$  at the equilibrium swollen state. (b) The normalized thickness of the polymer network  $h/H$  as a function of the dimensionless square root of time  $t^{1/2}D_1^{1/2}/H$  for  $k_h^2/D_1 \rightarrow \infty$ . The dashed line at  $t^{1/2}D_1^{1/2}/H = 0$  corresponds to an asymptotic self-similar solution at short time. The horizontal dashed line corresponds to the equilibrium swollen state of the polymer network. The calculation is based on physical parameter values include  $N = 4.27 \times 10^{24} \text{ m}^{-3}$ ,  $\chi = 0.41$ ,  $T = 293 \text{ K}$ ,  $\nu = 3.0 \times 10^{-29} \text{ m}^3$ , and  $\lambda_\infty = 9.95$  (Yuk et al., 2019).

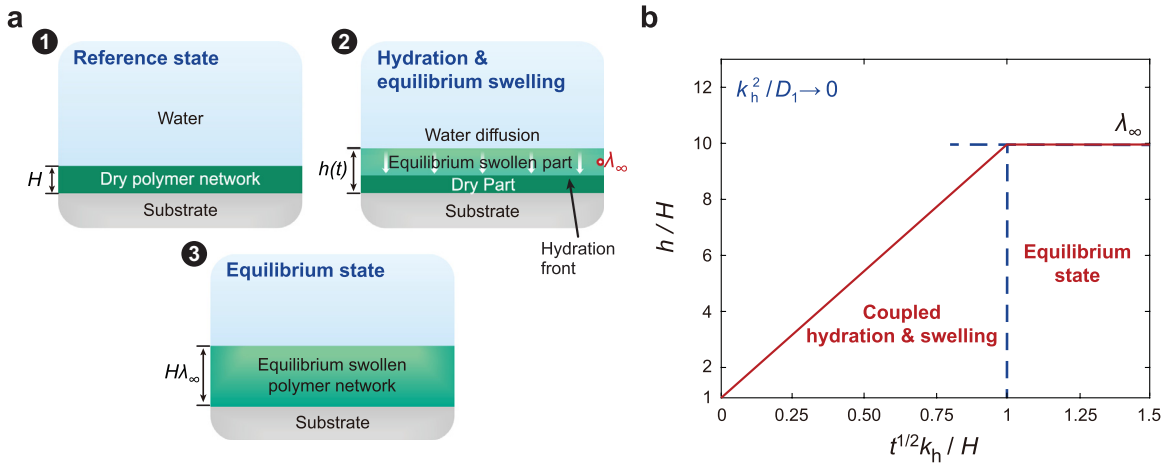


**Fig. 6.** A limiting case of an infinitesimal hydration speed, in which the kinetics of water transportation is governed by coupled hydration and swelling. (a) Schematic illustrations for the swelling of a dry polymer network with an infinitesimal hydration coefficient  $k_h$  ( $k_h^2/D_1 \rightarrow 0$ ). After the introduction of water, the polymer network undergoes the coupled hydration and swelling process until reaching the equilibrium swollen state with a thickness of  $H\lambda_\infty$ . (b) The normalized thickness of the polymer network  $h/H$  as a function of the dimensionless square root of time  $t^{1/2}k_h/H$  for  $k_h^2/D_1 \rightarrow 0$ , where  $\lambda_\infty = 9.95$  as in Fig. 5b.

top surface and the polymer network swells in the same manner as a wet hydrogel film. Fig. 5b shows the increase in the normalized thickness of the polymer network  $h/H$  as a function of the dimensionless square root of time  $t^{1/2}D_1^{1/2}/H$ . At the beginning of the pure swelling stage, the increase in the thickness  $\Delta h$  has a linear relation with  $t^{1/2}$  according to a self-similar solution (Bouklas and Huang, 2012; Yoon et al., 2010):

$$\frac{h}{H} = \frac{2}{\sqrt{\pi}}(\lambda_\infty - 1)\frac{\sqrt{tD_1}}{H} + 1 \tag{3.1}$$

which corresponds to the oblique dashed line in Fig. 5b. Additionally, the normalized thickness of the polymer network is bounded by the equilibrium swelling ratio  $\lambda_\infty$ .

The second limiting case corresponds to an infinitesimal hydration speed, i.e.,  $k_h^2/D_1 \rightarrow 0$ . Under this condition, the polymer network only undergoes the coupled hydration and swelling process. As illustrated in Fig. 6a, as the hydration front advances towards the substrate, the hydrated part always reaches the equilibrium swollen state. We can quantitatively un-

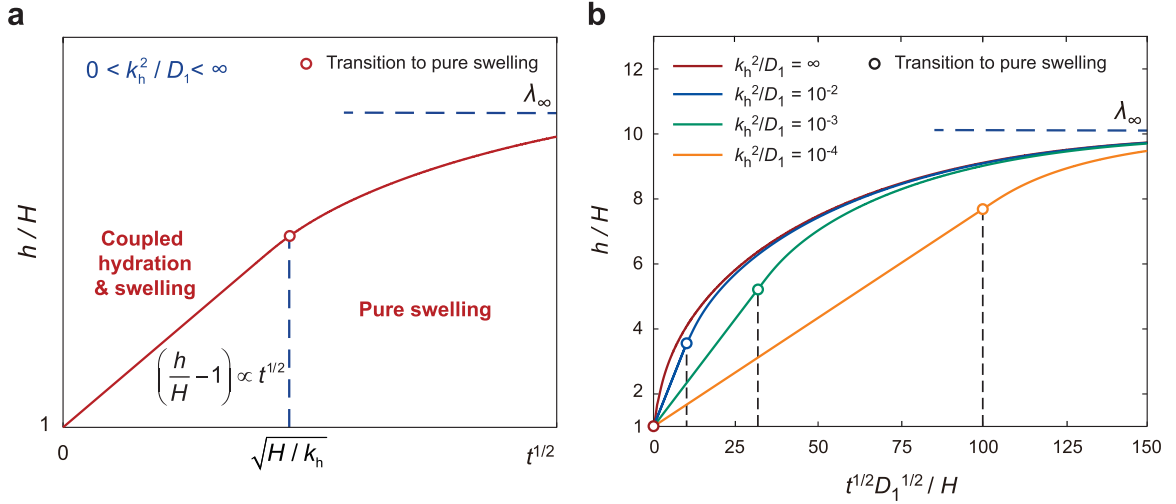


**Fig. 7.** (a) Normalized thickness of the polymer network  $h/H$  as a function of  $t^{1/2}$  for arbitrary  $0 < k_h^2/D_1 < \infty$ . The vertical dashed line denotes the transition from the coupled hydration and swelling stage to the pure swelling stage.  $(h/H - 1)$  is proportional to  $t^{1/2}$  in the coupled hydration and swelling stage. (b) The normalized thickness of the polymer network  $h/H$  as a function of the dimensionless square root of time  $t^{1/2}D_1^{1/2}/H$  for varying  $k_h^2/D_1$ . The vertical dashed line denotes the transition from the coupled hydration and swelling stage to the pure swelling stage. Physical parameters take the same values as in Fig. 5b.

derstand this phenomenon by inserting  $k_h = 0$  into Eq. (2.25)

$$\frac{d^2\lambda}{d\bar{X}^2} + f(\lambda) \left( \frac{d\lambda}{d\bar{X}} \right)^2 = 0 \quad (3.2)$$

Eq. (3.2) can be solved with the boundary conditions in Eq. (2.26), which yields  $\lambda(0 < \bar{X} < 1) = \lambda_h = \lambda_\infty$ . Thus, the hydrated part keeps in the equilibrium swollen state due to the extremely slow hydration process. Also, the normalized thickness of the polymer network  $h/H$  follows a linear relation with the dimensionless square root of time  $t^{1/2}k_h/H$ , namely

$$\frac{h(t)}{H} = (\lambda_\infty - 1) \frac{k_h}{H} t^{1/2} + 1 \quad (3.3)$$

with a slope of  $(\lambda_\infty - 1)$  (Fig. 6b).

#### 4. Numerical results for general situations

In Section 3, we discussed two limiting cases, in which either hydration or pure swelling dominates the kinetics. However, the dimensionless quantity  $k_h^2/D_1$  generally lies between zero and infinity for common dry polymer networks. Thus, both the coupled hydration and swelling stage and the pure swelling stage exist.

In the coupled hydration and swelling stage, the current thickness of the polymer  $h(t)$  can be expressed as

$$h(t) = \left( \int_0^1 \lambda(\bar{X}) d\bar{X} \right) k_h t^{1/2} + \left( H - k_h t^{1/2} \right) = \left( \int_0^1 \lambda(\bar{X}) d\bar{X} - 1 \right) k_h t^{1/2} + H \quad (4.1)$$

where the term  $\int_0^1 \lambda(\bar{X}) d\bar{X}$  gives the average swelling ratio in the hydrated part. Because  $\int_0^1 \lambda(\bar{X}) d\bar{X}$  does not depend on time, the current thickness has a linear relation with  $t^{1/2}$  in the coupled hydration and swelling stage (Fig. 7a). After the polymer network becomes fully hydrated at  $t = \sqrt{H/k_h}$ , the current thickness  $h(t)$  in the pure swelling stage can be expressed as

$$h(t) = \int_0^H \lambda(X, t) dX \quad (4.2)$$

which can be evaluated by numerically solving Eqs. (2.14) – (2.15) and (2.30) – (2.31).

Fig. 7b shows the normalized thickness of the polymer network  $h/H$  as a function of the dimensionless square root of time  $t^{1/2}D_1^{1/2}/H$  for  $k_h^2/D_1 = 10^{-2}$ ,  $10^{-3}$ , and  $10^{-4}$ . The limiting condition  $k_h^2/D_1 = \infty$  is also shown in Fig. 7b for comparison.

The influence of  $k_h^2/D_1$  on the overall kinetics can be analyzed by comparing the curves in Fig. 7. As  $k_h^2/D_1$  decreases, on one hand, it requires a longer time for the hydration process to finish; on the other hand, the transiting point to pure swelling corresponds to a greater thickness  $h$  of the polymer network. This phenomenon can be explained as the following: If the thickness  $H$  of the polymer network is held constant, a lower  $k_h$  corresponds to a greater transiting time  $\sqrt{H/k_h}$ .

Consequently, more water can diffuse into the polymer network and lead to a higher swelling ratio. Moreover, lower hydration speed induces a reduction in the swelling speed of the polymer network, which is especially the case for a very low hydration coefficient (e.g.,  $k_h^2/D_1 = 10^{-4}$  in Fig. 7b).

## 5. Experimental validation of the theory

In this section, we experimentally verify the theoretical model developed in Section 2. A dry chitosan-based polymer network is chosen as the model polymer network. To make numerical predictions for the hydration and swelling of the polymer network, a model requires the thermodynamic parameters  $N$ ,  $\chi$  and the kinetic parameters  $D_1$ ,  $k_h$  of the polymer. Given the above parameters, the increase in the thickness of the polymer network over time is numerically calculated, which is further compared with the experimental results for the swelling of the dry polymer network.

The thermodynamic parameters  $N$  and  $\chi$  were measured in a previous paper (Yuk et al., 2019). Herein, we recapitulate the methods employed. To determine  $N$ , the shear modulus  $G_0$  is measured for the as-prepared polymer network as a hydrogel, and then,  $N$  is calculated from (Bouklas and Huang, 2012)

$$G_0 = \frac{1}{\lambda_0} N k_B T \quad (5.1)$$

where  $\lambda_0$  is the swelling ratio of the as-prepared polymer network.

Next, a free-swelling experiment for the as-prepared polymer network was carried out to determine  $\chi$  (Yuk et al., 2019). During the free-swelling experiment, the polymer network reached an unconstrained equilibrium swelling ratio  $\lambda_\infty$  in all dimensions. Once  $\lambda_\infty$  is measured,  $\chi$  can be calculated based on the expression for the Cauchy stress in the unconstrained swelling process (Bouklas and Huang, 2012)

$$\sigma = N k_B T (\lambda_\infty^{-1} - \lambda_\infty^{-3}) + \frac{k_B T}{\nu} [\ln(1 - \lambda_\infty^{-3}) + \lambda_\infty^{-3} + \chi \lambda_\infty^{-6}] \quad (5.2)$$

where  $\sigma = 0$  in the equilibrium swollen state. With  $\chi$  measured, the equilibrium swelling ratio  $\lambda_\infty$  for the constrained swelling experiment can be further predicted based on Eq. (2.10). The physical parameters for the chitosan-based polymer network were calculated to be  $N = 4.27 \times 10^{24} \text{ m}^{-3}$ ,  $\chi = 0.41$  (Yuk et al., 2019), which give  $\lambda_\infty = 9.95$ .

To measure the diffusivity  $D_1$ , we carry out swelling experiments for an as-prepared fully hydrated polymer network that is bonded to a solid substrate. Because the as-prepared polymer network has a stretching ratio of  $\lambda_0$  in all dimensions relative to the reference state, its initial thickness is  $H\lambda_0$  (Fig. 8a). At time  $t = 0$ , the polymer network is soaked into a water bath and undergoes the constrained swelling process. The thickness of the polymer network  $h(t)$  is recorded as a function of time. Given the thermodynamic parameters of the polymer network, we can also numerically solve the variation in  $h$  over time by assuming a specific value for the diffusivity  $D_1$ . By comparison between the experimental and numerical results, a fitted diffusivity of  $5.15 \times 10^9 \text{ m}^2 \text{ s}^{-1}$  is obtained for the chitosan-based polymer network (Fig. 8a).

For the measurement of the hydration coefficient  $k_h$ , we recall that the position of the hydration front is linearly related to the square root of time, i.e.,  $X_h = k_h t^{1/2}$ . Consequently, we can measure the time  $t_p$  required for the hydration front to penetrate through dry polymer networks with varying thicknesses, and then fit  $k_h$  based on the relation  $H = k_h t_p^{1/2}$ . The experimental design is illustrated in Fig. 8b. A layer of dry fluorescein is introduced to the bottom surface of a dry polymer network (with a thickness of  $H$ ) as the hydration indicator. At time  $t = 0$ , water is introduced to the top surface of the polymer network, and the hydration front starts to advance through the polymer network. When the dry polymer network becomes fully hydrated, the fluorescein layer at the bottom surface also starts to be hydrated. The penetration time  $t_p$  is recorded once the green fluorescence appears. By repeating the experiments for dry polymer networks with varying thicknesses, a fitted hydration coefficient  $k_h$  of  $9.31 \times 10^{-6} \text{ m s}^{-1/2}$  is obtained for the chitosan-based polymer networks.

After measuring the diffusivity  $D_1$  and the hydration coefficient  $k_h$ , the last step is to validate the theoretical model developed in Section 2. As shown in Fig. 8c, we bond a dry polymer network to a rigid substrate and measure the variation of thickness  $h$  over time after soaking it into a water bath. The experimentally measured and numerically predicted thicknesses of the polymer network are plotted as functions of the square root of time in Fig. 8c. In addition, the boundary between the coupled hydration and swelling stage and the pure swelling stage can be identified in the plot. With independently measured physical parameters such as  $k_h$  and  $D_1$ , it is clear that our theoretical model can provide relatively accurate predictions for the swelling of a dry polymer network in contact with water. Consequently, we can further employ the theoretical model to quantitatively understand the drying of interfacial water by dry polymer networks.

## 6. Discussions

### 6.1. Guideline for the design of dry adhesives for wet adhesion

With the quantitative understanding of the hydration and swelling kinetics of dry polymer networks, we can further establish a guideline for the design of dry adhesives that can achieve rapid and strong wet adhesion. The guideline includes an

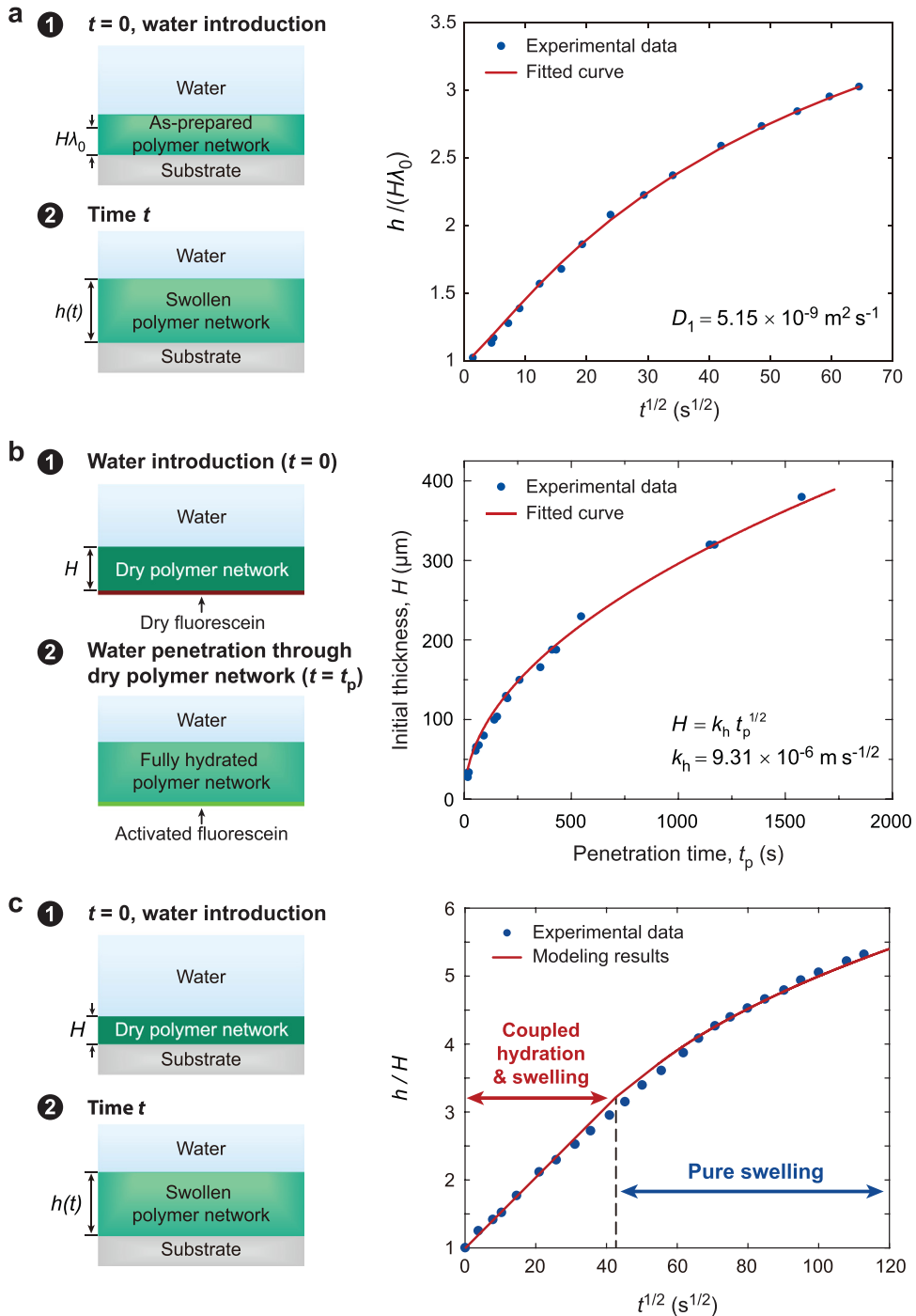


**Fig. 8.** Experimental validation of the coupled hydration and swelling model by using chitosan-based polymer networks. (a) Measurement of the diffusivity  $D_1$  for an as-prepared polymer network. The as-prepared polymer network is bonded to a solid substrate with an initial thickness of  $H\lambda_0$ . At  $t = 0$ , it starts to undergo the constrained swelling process. The normalized thickness of the polymer network,  $h/H\lambda_0$ , is plotted as a function of the square root of time, from which a fitted diffusivity of  $5.15 \times 10^{-9} \text{ m}^2 \text{ s}^{-1}$  can be obtained. (b) Measurement of the hydration coefficient  $k_h$  for the dry polymer network. As the hydration indicator, a layer of dry fluorescein is applied to the bottom surface of a dry polymer network with a thickness of  $H$ . At  $t = 0$ , water is introduced to the top surface of the polymer network. At  $t = t_p$ , water penetrates through the polymer network and activates the fluorescein. Based on this experiment, a fitted hydration coefficient  $k_h$  of  $9.31 \times 10^{-6} \text{ m s}^{-1/2}$  is obtained. (c) Experimental validation of the coupled hydration and constrained swelling model. A dry polymer network with a thickness of  $H$  is bonded to a rigid substrate. At  $t = 0$ , the polymer network starts to undergo the coupled hydration and swelling stage, which is followed by the pure swelling stage. The normalized thickness of the polymer network,  $h/H$ , is plotted as a function of the square root of time for both experimental and numerical results. The dry polymer network has an initial thickness of  $400 \mu\text{m}$ .

optimized capability to remove interfacial water within a certain amount of time and the tough stable bonding of polymer networks to wet surfaces.

Rapid removal of interfacial water can be achieved by tuning physical and geometric parameter values for the dry polymer networks, including diffusivity  $D_1$ , hydration coefficient  $k_h$ , equilibrium swelling ratio  $\lambda_\infty$ , and the thickness of the dry polymer network  $H$ . Additionally, the time for the removal of interfacial water also depends on the thickness of interfacial water  $H_{\text{water}}$ , and thus

$$t_{\text{water}} = t(D_1, k_h, \lambda_\infty, H, H_{\text{water}}) \quad (6.1)$$

where  $t_{\text{water}}$  is the amount of time for the absorption of interfacial water. To achieve a shorter  $t_{\text{water}}$ , higher values of  $k_h$  and  $D_1$  are preferred, as they imply a higher speed of water transportation within the polymer networks. A higher value of  $\lambda_\infty$  implies the dry polymer network is capable of removing a higher amount of interfacial water. Furthermore, a higher dry thickness  $H$  is preferable for both absorbing more water and drying more rapidly.

To achieve fast adhesion of the polymer networks on the substrate, we can introduce reversible bonds such as hydrogen bonds and electrostatic interactions with the substrate, which take effect upon removal of the interfacial water. Then the time for adhesion formation is equal to  $t_{\text{water}}$  (Yuk et al., 2019). For stable adhesion over the long term, we need more stable linkages between the adhesive and the substrate than the reversible bonds. These stable linkages are usually achieved by chemical crosslinking of the polymer networks on the substrate, which occurs simultaneously with or shortly after the reversible bonds (Yuk et al., 2016a, 2019). Overall, the reversible bonds and chemical crosslinking of the polymer network on the substrate give the intrinsic interfacial toughness  $\Gamma_0$ .

To achieve tough adhesion, the adhesive should be composed of a tough and dissipative polymer network. Thus, as the adhesive is detached from the substrate, a significant amount of mechanical energy can be dissipated due to the large deformation of the polymer network, which is quantified as the contribution of the bulk dissipation to the interfacial toughness  $\Gamma_D$  (Yuk et al., 2016b; Zhang et al., 2017; Zhao, 2014). High values of  $\Gamma_0$  and  $\Gamma_D$  give rise to a high interfacial toughness of adhesion  $\Gamma$ , namely

$$\Gamma = \Gamma_0(t > t_{\text{water}}) + \Gamma_D \quad (6.2)$$

in which  $t > t_{\text{water}}$  indicates that the formation of the adhesion at least takes the time of  $t_{\text{water}}$ .

## 6.2. Adhesion time for the diffusion-based and dry-crosslinking mechanisms

The diffusion-based mechanism relies on the diffusion of adhesive molecules across the interfacial water layer to form wet adhesion. The diffusivity of the adhesive molecules in the form of polymers chains can be expressed as (Rubinstein and Colby, 2003)

$$D_R = \frac{D_{\text{mon}}}{n} \quad (6.3)$$

$$D_Z = \frac{D_{\text{mon}}}{n^\nu} \quad (6.4)$$

where  $D_R$  and  $D_Z$  are the diffusivities of the adhesive polymer chains in water according to the Rouse and Zimm models (Rouse, 1953; Zimm, 1956), respectively,  $D_{\text{mon}}$  is the diffusivity of a Kuhn monomer on the polymer chain,  $n$  is the number of Kuhn monomers per polymer chain, and  $\nu$  is the scaling exponent for the polymer size. The concentration of the adhesive polymer chains in the interfacial water layer determines which model the diffusion of the polymer chains will follow. A semi-dilute solution of the adhesive polymer chains will follow the Rouse model, and a dilute solution will follow the Zimm model (Rubinstein and Colby, 2003). The value of  $n$  can range from hundreds to millions for common polymers, and the value of  $\nu$  is 0.5 for ideal polymer chains (i.e., polymer chains in theta solvent) (Rubinstein and Colby, 2003).

Therefore, the time for an adhesive polymer chain to diffuse across the interfacial water layer can be expressed as

$$t_R = t_{\text{mon}}n \quad (6.5)$$

$$t_Z = t_{\text{mon}}n^\nu \quad (6.6)$$

where  $t_R$  and  $t_Z$  are the diffusion time according to the Rouse and Zimm models (Rouse, 1953; Zimm, 1956), respectively, and  $t_{\text{mon}}$  is the diffusion time for the corresponding Kuhn monomer.

Since the diffusivity of water in hydrated polymer networks  $D_1$  and the diffusivity of Kuhn monomers in water  $D_{\text{mon}}$  are on the same order, the absorption time of water  $t_{\text{water}}$  (given the relatively fast hydration condition) and the diffusion time of Kuhn monomers  $t_{\text{mon}}$  should be on the same order. Therefore, the diffusion time of adhesive polymer chains in the diffusion-based mechanism  $t_R$  or  $t_Z$  can be  $n$  or  $n^\nu$  times of the absorption time of water  $t_{\text{water}}$  in the dry-crosslinking mechanism according to the Rouse or Zimm model, respectively.

## 7. Concluding remarks

Interfacial water poses a challenge for the formation of fast and robust adhesion between wet surfaces. To eliminate the separation effect of the interfacial water, the dry-crosslinking mechanism has been proposed to dry the interfacial water for rapid and strong wet adhesion. However, the kinetics of drying interfacial water in the dry-crosslinking mechanism have not been quantitatively explained. In this work, we develop a theoretical model to understand the physics and mechanics of hydration and swelling of dry polymer networks for drying interfacial water. The drying process contains two stages, namely a coupled hydration and swelling stage and a pure swelling stage. An advancing hydration front divides the polymer network into a hydrated swelling part and a dry part during the coupled hydration and swelling stage. Our one-dimensional theoretical model can quantify the hydration and swelling processes of dry polymer networks. A dimensionless quantity  $k_h^2/D_1$  characterizes the ratio of hydration and swelling speeds. Correspondingly, the hydration and swelling kinetics vary significantly as  $k_h^2/D_1$  varies from zero to infinity. A set of hydration and swelling experiments are performed with dry chitosan-based polymer networks, which agree well with theoretical predictions for the swelling profile, validating the effectiveness of our theoretical model. Our theoretical model can facilitate the rationally-guided design of dry adhesives for wet adhesion. In addition, this work provides a foundation for further studies on the coupled hydration and inhomogeneous swelling behaviors of dry polymeric materials with more general form factors and applications.

## Declaration of Competing Interest

The authors declare that they have no known competing financial interests or personal relationships that could have appeared to influence the work reported in this paper.

## CRediT authorship contribution statement

**Xinyu Mao:** Conceptualization, Methodology, Formal analysis, Investigation, Writing - original draft, Writing - review & editing. **Hyunwoo Yuk:** Conceptualization, Methodology, Investigation, Writing - original draft, Writing - review & editing, Funding acquisition. **Xuanhe Zhao:** Conceptualization, Methodology, Writing - original draft, Writing - review & editing, Supervision, Funding acquisition.

## Acknowledgments

This work was supported by the NSF (EFMA-1935291) and the U.S. Army Research Office through the Institute for Soldier Nanotechnologies at Massachusetts Institute of Technology (W911NF-13-D-0001).

## Appendix A. Preparation of chitosan-based polymer network

**Materials.** For the polyacrylic acid-chitosan double-network hydrogel, acrylic acid (Sigma-Aldrich) and chitosan (Sigma-Aldrich) were used. Gelatin methacryloyl (GelMA, Sigma-Aldrich) was used as the crosslinker and  $\alpha$ -ketoglutaric acid (Sigma-Aldrich) was used as the photo-initiator. *N*-Succinimidyl acrylate (Sigma-Aldrich) was used to couple the polymer network with the adherends.

**Methods.** The chitosan-based polymer network was prepared based on the previously reported protocol (Yuk et al., 2019). Dissolve 30 w/w% acrylic acid, 2 w/w% chitosan, 0.1 w/w% gelatin methacryloyl, 1 w/w% *N*-Succinimidyl acrylate, and 0.5 w/w%  $\alpha$ -ketoglutaric acid in deionized water. The solution is poured into a glass mold and then cured in an ultraviolet (UV) chamber (284 nm, 10 W power) for 60 min. The as-prepared polymer network is then hanged in a fume hood to guarantee isotropic drying in all dimensions. Finally, the dry polymer network is bonded to a rigid acrylic substrate by using cyanoacrylate glue (Krazy Glue™) for constrained swelling tests.

## Appendix B. Convergence of the numerical method for the coupled hydration and swelling model

In Section 2, we assumed that the dry part corresponds to an infinitesimal diffusivity, i.e.,  $D_2 \rightarrow 0$ . Yet a finite  $D_2$  should always be assigned for solving Eq. (2.27) numerically. Herein, we prove that the numerical solution will converge as  $D_2$  approaches zero. Thus, assuming a  $D_2$  that is small enough can guarantee accurate numerical results.

Given the measured parameter values for the chitosan-based polymer network ( $D_1$  and  $k_h$ ), we calculate the distribution of the swelling ratio  $\lambda$  across the hydrated part during the coupled hydration and swelling process. The dependence of  $\lambda$  on the dimensionless coordinate  $\bar{X}$  for varying  $D_2/D_1$  is shown in Fig. B.1. The  $\lambda - \bar{X}$  curve elevates and converges as  $D_2/D_1 \rightarrow 0$ . For  $D_2/D_1 = 10^{-3}$ ,  $10^{-4}$ , and  $10^{-5}$ , no significant difference can be found for the  $\lambda - \bar{X}$  curves. Specifically, the critical swelling ratio  $\lambda_h$  converges to 2.26 as  $D_2/D_1$  decreases to  $10^{-5}$ . Based on Eq. (2.1), a critical water concentration  $C_h$  of  $6.97 \times 10^4$  mol/m<sup>3</sup> (with respect to reference state) and  $c_h$  of  $3.09 \times 10^4$  mol/m<sup>3</sup> (with respect to the current state) are



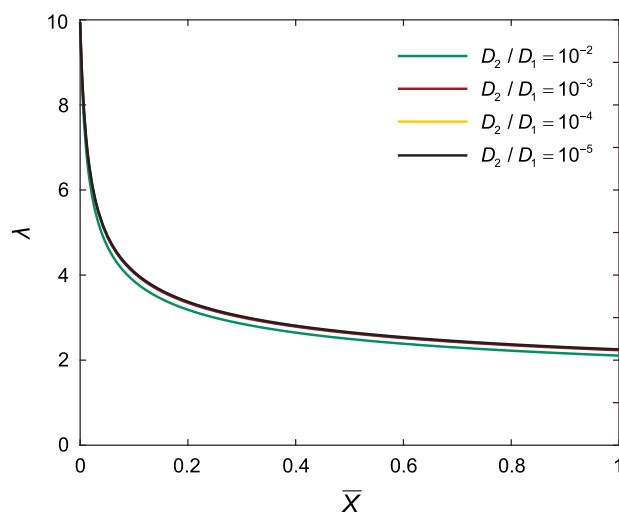


**Fig. B. 1.** Distribution of the swelling ratio  $\lambda$  across the hydrated part in the coupled hydration and swelling model for varying ratios of  $D_2/D_1$ . The measured parameters  $D_1$  and  $k_h$  are held constant.

calculated. Therefore, Fig. B.1. proves the effectiveness of our numerical procedure to acquire accurate results for the coupled hydration and swelling process.

## References

- Alfrey Jr., T., Gurnee, E.F., Lloyd, W.G., 1966. Diffusion in glassy polymers. *J. Polym. Sci., C Polym. Symp.* 12, 249–261.
- Anand, L., Ames, N.M., Srivastava, V., Chester, S.A., 2009. A thermo-mechanically coupled theory for large deformations of amorphous polymers. Part I: Formulation. *Int. J. Plast.* 25, 1474–1494.
- Annabi, N., Yue, K., Tamayol, A., Khademhosseini, A., 2015. Elastic sealants for surgical applications. *Eur. J. Pharm. Biopharm.* 95, 27–39.
- Bartlett, M.D., Croll, A.B., King, D.R., Paret, B.M., Irschick, D.J., Crosby, A.J., 2012. Looking beyond fibrillar features to scale gecko-like adhesion. *Adv. Mater.* 24, 1078–1083.
- Bouklas, N., Huang, R., 2012. Swelling kinetics of polymer gels: comparison of linear and nonlinear theories. *Soft Matter* 8, 8194–8203.
- Bouklas, N., Landis, C.M., Huang, R., 2015. A nonlinear, transient finite element method for coupled solvent diffusion and large deformation of hydrogels. *J. Mech. Phys. Solids* 79, 21–43.
- Buckingham, E., 1914. On physically similar systems; illustrations of the use of dimensional equations. *Phys. Rev.* 4, 345.
- Chaudhury, M.K., 1996. Interfacial interaction between low-energy surfaces. *Mater. Sci. Eng. R Reports* 16, 97–159.
- Chester, S.A., Anand, L., 2010. A coupled theory of fluid permeation and large deformations for elastomeric materials. *J. Mech. Phys. Solids* 58, 1879–1906.
- Chester, S.A., Di Leo, C.V., Anand, L., 2015. A finite element implementation of a coupled diffusion-deformation theory for elastomeric gels. *Int. J. Solids Struct.* 52, 1–18.
- Chung, H., Grubbs, R.H., 2012. Rapidly cross-linkable DOPA containing terpolymer adhesives and PEG-based cross-linkers for biomedical applications. *Macromolecules* 45, 9666–9673.
- Chung, J.Y., Chaudhury, M.K., 2005. Soft and hard adhesion. *J. Adhes.* 81, 1119–1145.
- Comyn, J., 2012. *Polymer Permeability*. Springer, Dordrecht.
- Crank, J., 1979. *The Mathematics of Diffusion*. Oxford university press, London.
- Crank, J., 1953. A theoretical investigation of the influence of molecular relaxation and internal stress on diffusion in polymers. *J. Polym. Sci.* 11, 151–168.
- Crank, J., 1951. Diffusion in media with variable properties. Part III.—Diffusion coefficients which vary discontinuously with concentration. *Trans. Faraday Soc.* 47, 450–461.
- Creton, C., 2003. Pressure-sensitive adhesives: an introductory course. *MRS Bull* 28, 434–439.
- Doi, M., 2009. Gel dynamics. *J. Phys. Soc. Japan* 78, 52001.
- Flory, P.J., 1953. *Principles of polymer chemistry*. Cornell University Press, Ithaca, NY.
- Flory, P.J., 1942. Thermodynamics of high polymer solutions. *J. Chem. Phys.* 10, 51–61.
- Flory, P.J., Rehner Jr., J., 1943. Statistical mechanics of cross-linked polymer networks. II. *J. Chem. Phys.* 11, 521–526.
- Frisch, H.L., Wang, T.T., Kwei, T.K., 1969. Diffusion in glassy polymers. II. *J. Polym. Sci. Part A-2 Polym. Phys.* 7, 879–887.
- Hartley, G.S., 1946. Diffusion and swelling of high polymers. Part I.—The swelling and solution of a high polymer solid considered as a diffusion process. *Trans. Faraday Soc.* 42, B006–B011.
- Hohlfeld, E., Mahadevan, L., 2012. Scale and nature of sulcification patterns. *Phys. Rev. Lett.* 109, 25701.
- Hong, W., Zhao, X., Suo, Z., 2009. Formation of creases on the surfaces of elastomers and gels. *Appl. Phys. Lett.* 95, 111901.
- Hong, W., Zhao, X., Zhou, J., Suo, Z., 2008. A theory of coupled diffusion and large deformation in polymeric gels. *J. Mech. Phys. Solids* 56, 1779–1793.
- Huggins, M.L., 1941. Solutions of long chain compounds. *J. Chem. Phys.* 9, 440.
- Ji, S., Ding, J., 2002. The wetting process of a dry polymeric hydrogel. *Polym. J.* 34, 267.
- Kelley, F.N., Bueche, F., 1961. Viscosity and glass temperature relations for polymer-diluent systems. *J. Polym. Sci.* 50, 549–556.
- Kwei, T.K., Zupko, H.M., 1969. Diffusion in glassy polymers. I. *J. Polym. Sci. Part A-2 Polym. Phys.* 7, 867–877.
- Lasky, R.C., Kramer, E.J., Hui, C.-Y., 1988. Temperature dependence of case II diffusion. *Polymer (Guildf)* 29, 1131–1136.
- Lee, B.P., Messersmith, P.B., Israelachvili, J.N., Waite, J.H., 2011. Mussel-inspired adhesives and coatings. *Annu. Rev. Mater. Res.* 41, 99–132.
- Lee, L.-H., 2013. *Fundamentals of Adhesion*. Springer Science & Business Media, New York.
- Li, J., Celiz, A.D., Yang, J., Yang, Q., Wamala, I., Whyte, W., Seo, B.R., Vasilyev, N.V., Vlassak, J.J., Suo, Z., 2017. Tough adhesives for diverse wet surfaces. *Science* 357, 378–381.
- Long, R., Hui, C.-Y., 2012. Axisymmetric membrane in adhesive contact with rigid substrates: Analytical solutions under large deformation. *Int. J. Solids Struct.* 49, 672–683.

- Long, R., Shull, K.R., Hui, C.-Y., 2010. Large deformation adhesive contact mechanics of circular membranes with a flat rigid substrate. *J. Mech. Phys. Solids* 58, 1225–1242.
- Meddahi-Pellé, A., Legrand, A., Marcellan, A., Louedec, L., Letourneur, D., Leibler, L., 2014. Organ repair, hemostasis, and in vivo bonding of medical devices by aqueous solutions of nanoparticles. *Angew. Chemie Int. Ed.* 53, 6369–6373.
- Peppas, N.A., Colombo, P., 1997. Analysis of drug release behavior from swellable polymer carriers using the dimensionality index. *J. Control. Release* 45, 35–40.
- Petrone, L., Kumar, A., Sutanto, C.N., Patil, N.J., Kannan, S., Palaniappan, A., Amini, S., Zappone, B., Verma, C., Miserez, A., 2015. Mussel adhesion is dictated by time-regulated secretion and molecular conformation of mussel adhesive proteins. *Nat. Commun.* 6, 8737.
- Quinn, J.V., 2005. *Tissue adhesives in clinical medicine*. Decker Inc., Hamilton.
- Rose, S., PrevotEAU, A., Elzière, P., Hourdet, D., Marcellan, A., Leibler, L., 2014. Nanoparticle solutions as adhesives for gels and biological tissues. *Nature* 505, 382.
- Rouse Jr, P.E., 1953. A theory of the linear viscoelastic properties of dilute solutions of coiling polymers. *J. Chem. Phys.* 21, 1272–1280.
- Rubinstein, M., Colby, R.H., 2003. *Polymer physics*. Oxford university press, New York.
- Thomas, N.L., Windle, A.H., 1982. A theory of case II diffusion. *Polymer* 23, 529–542.
- Waite, J.H., 1987. Nature's underwater adhesive specialist. *Int. J. Adhes. Adhes.* 7, 9–14.
- Wang, D.-A., Varghese, S., Sharma, B., Strehin, I., Fermanian, S., Gorham, J., Fairbrother, D.H., Cascio, B., Elisseeff, J.H., 2007. Multifunctional chondroitin sulphate for cartilage tissue–biomaterial integration. *Nat. Mater.* 6, 385.
- Wang, T.T., Kwei, T.K., Frisch, H.L., 1969. Diffusion in glassy polymers. III. *J. Polym. Sci. Part A-2 Polym. Phys.* 7, 2019–2028.
- Windle, A.H., 1985. Case II sorption. In: *Polymer Permeability*. Springer, pp. 75–118.
- Yang, J., Bai, R., Chen, B., Suo, Z., 2019. Hydrogel adhesion: A supramolecular synergy of chemistry, topology, and mechanics. *Adv. Funct. Mater.*, 1901693.
- Yang, J., Bai, R., Suo, Z., 2018. Topological adhesion of wet materials. *Adv. Mater.* 30, 1800671.
- Yoon, J., Cai, S., Suo, Z., Hayward, R.C., 2010. Poroelastic swelling kinetics of thin hydrogel layers: comparison of theory and experiment. *Soft Matter* 6, 6004–6012.
- Yuk, H., Lin, S., Ma, C., Takaffoli, M., Fang, N.X., Zhao, X., 2017. Hydraulic hydrogel actuators and robots optically and sonically camouflaged in water. *Nat. Commun.* 8, 14230.
- Yuk, H., Varela, C.E., Nabzdyk, C.S., Mao, X., Padera, R.F., Roche, E.T., Zhao, X., 2019. Dry double-sided tape for adhesion of wet tissues and devices. *Nature* 575, 169–174.
- Yuk, H., Zhang, T., Lin, S., Parada, G.A., Zhao, X., 2016a. Tough bonding of hydrogels to diverse non-porous surfaces. *Nat. Mater.* 15, 190.
- Yuk, H., Zhang, T., Parada, G.A., Liu, X., Zhao, X., 2016b. Skin-inspired hydrogel–elastomer hybrids with robust interfaces and functional microstructures. *Nat. Commun.* 7, 12028.
- Zhang, T., Yuk, H., Lin, S., Parada, G.A., Zhao, X., 2017. Tough and tunable adhesion of hydrogels: experiments and models. *Acta Mech. Sin.* 33, 543–554.
- Zhao, X., 2014. Multi-scale multi-mechanism design of tough hydrogels: building dissipation into stretchy networks. *Soft Matter* 10, 672–687.
- Zhao, Y., Wu, Y., Wang, L., Zhang, M., Chen, X., Liu, M., Fan, J., Liu, J., Zhou, F., Wang, Z., 2017. Bio-inspired reversible underwater adhesive. *Nat. Commun.* 8, 2218.
- Zimm, B.H., 1956. Dynamics of polymer molecules in dilute solution: viscoelasticity, flow birefringence and dielectric loss. *J. Chem. Phys.* 24, 269–278.